THE JOURNAL OF PHYSICAL CHEMISTRY A

Article

pubs.acs.org/JPCA

Hygroscopicity of Organic Compounds as a Function of Carbon Chain Length and Carboxyl, Hydroperoxy, and Carbonyl Functional Groups

Sarah Suda Petters,[*,†] Demetrios Pagonis,[‡] Megan S. Claflin,[‡] Ezra J. T. Levin,[†] Markus D. Petters,[§] Paul J. Ziemann,[‡] and Sonia M. Kreidenweis[†]

[†]Department of Atmospheric Science, Colorado State University, Fort Collins, Colorado 80523-1371, United States

[‡]Department of Chemistry and Biochemistry, University of Colorado at Boulder, Boulder, Colorado 80309-0216, United States

[§]Department of Marine Earth and Atmospheric Sciences, North Carolina State University, Raleigh, North Carolina 27695-8208, United States

Supporting Information

ABSTRACT: The albedo and microphysical properties of clouds are controlled in part by the hygroscopicity of particles serving as cloud condensation nuclei (CCN). Hygroscopicity of complex organic mixtures in the atmosphere varies widely and remains challenging to predict. Here we present new measurements characterizing the CCN activity of pure compounds in which carbon chain length and the numbers of hydroperoxy, carboxyl, and carbonyl functional groups were systematically varied to establish the contributions of these groups to organic aerosol apparent hygroscopicity. Apparent hygroscopicity decreased with carbon chain length and increased with polar functional groups in the order carboxyl > hydroperoxy > carbonyl. Activation diameters at different supersaturations deviated from the −3/2 slope in log−log space predicted by Köhler theory, suggesting that water solubility limits CCN activity of particles composed of weakly functionalized organic compounds. Results are compared to a functional group contribution model that predicts CCN activity of organic compounds. The model performed well for most compounds but underpredicted the CCN activity of hydroperoxy groups. New best-fit hydroperoxy group/water interaction parameters were derived from the available CCN data. These results may help improve estimates of the CCN activity of ambient organic aerosols from composition data.

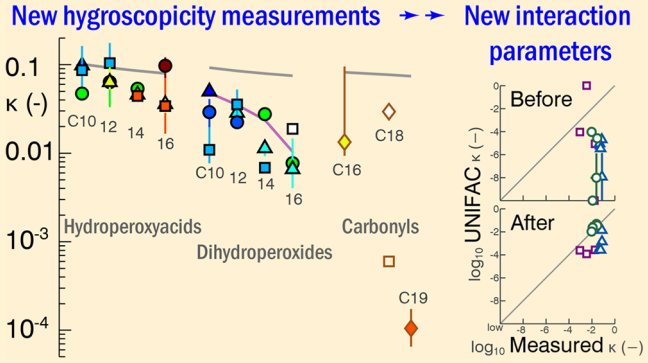

INTRODUCTION

Atmospheric aerosols participate in the formation of clouds by serving as cloud condensation nuclei (CCN),[1,2] affect the global radiative balance through direct and indirect effects,[3,4] and can be detrimental to the well-being of plants and animals.[5,6] Numerous organic compounds contribute to the aerosol mass in the atmosphere,[7,8] many of which are formed through secondary processes. Secondary organic aerosol (SOA) forms when volatile organic compounds are oxidized in the atmosphere, yielding low-volatility compounds that can condense.[9,10] Low-volatility compounds also form in aqueous phase reactions as dissolved organic compounds are oxidized in cloud droplets[11,12] or wet aerosols.[13,14] Because of the chemical complexity of SOA, the chemical evolution and properties of SOA in the atmosphere are often described by simplified metrics such as the elemental oxygen to carbon ratio (O:C),[15,16] the fraction of mass spectral fragment at mass-to-charge ratio 44 (f_{44}),[17] the change in H:C ratio relative to the O:C ratio,[18] or the average oxidation state of carbon.[19] The O:C ratio and f_{44} are both good predictors of the hygroscopicity of the organic fraction of aerosols in the atmosphere,[15−17] but the relationship with hygroscopicity is not linear and may vary greatly under different conditions,[20−23] demonstrating the need to include more detailed information such as molecular structure.

Many organic compounds present in SOA contribute to the hygroscopicity of the whole particle.[24,25] The hygroscopicity of each compound depends on the length of the carbon chain and the number and type of attached functional groups.[23] Aerosol water content can be predicted by chemical equilibrium models such as UNIFAC for arbitrary mixtures of organic functional groups in solution.[26] UNIFAC predictions of aerosol properties are widely used in the aerosol community[27−31] and also serve as the core component of a model we have developed to predict CCN activity from functional group composition and particle dry diameter[30] (hereafter referred to as the U-CCN model).

Received: May 1, 2017
Revised: June 13, 2017
Published: June 16, 2017

DOI: 10.1021/acs.jpca.7b04114
J. Phys. Chem. A 2017, 121, 5164−5174

UNIFAC is semiempirical, and thus measurements are necessary to constrain predictions.[28,29] Most single-component studies characterizing the CCN activity of organic aerosols have been limited to chemicals that are commercially available. Suitable data sets for fitting empirical UNIFAC interaction parameters remain limited due to the difficulty of synthesizing a large suite of compounds with targeted functional groups. Although the U-CCN model was previously validated against a database of published laboratory CCN measurements, that database had limited coverage for many functional groups that are important in atmospheric organic aerosols. This work aims to close the gap for carboxyl, hydroperoxy, and carbonyl functional groups, which are investigated by using organic synthesis to systematically vary the type and location of the functional group on the carbon backbone. The U-CCN model uses a UNIFAC core to predict water activity,[26] a functional group prediction of molar volume,[32] and a liquid−liquid phase equilibrium algorithm.[33] These are combined with traditional Köhler theory to predict CCN activity. The efficacy by which individual functional groups promote CCN activity is strongly tied to the water activity and solubility/miscibility for highly dilute solutions,[30] meaning that validation and tuning of UNIFAC group interaction parameters for the U-CCN model must be performed against actual CCN measurements. Therefore, this work primarily focuses on measurements of CCN activity, expressed in terms of the compound's hygroscopicity parameter, to improve the fidelity of the U-CCN model.

THEORY

Here the hygroscopicity parameter κ is used together with Köhler theory to describe CCN activation (eq 1) and aerosol water uptake in subsaturated relative humidity (eq 2):[24,34]

$$S_c(\kappa, D_d) = \max\left(\frac{D^3 - D_d^3}{D^3 - D_d^3(1-\kappa)} \exp\left(\frac{A}{D}\right)\right) \quad (1)$$

$$S(\kappa, G_f) = \frac{G_f^3 - 1}{G_f^3 - (1-\kappa)} \exp\left(\frac{A}{D_d G_f}\right) \quad (2)$$

where S_c is the critical water vapor supersaturation at CCN activation, D is the droplet diameter, D_d is the particle dry diameter, $A = 4\sigma M_w/(RT\rho_w)$ is the Kelvin diameter, σ is the surface tension of the air/solution interface, M_w is the molar mass of pure water, R is the universal gas constant, T is temperature, ρ_w is the density of pure water, S is the water vapor saturation ratio (relative humidity expressed as a fraction), and $G_f = D/D_d$ is the diameter growth factor. Throughout this work S_c is expressed as a percent: $s_c = (S_c - 1) \times 100\%$. By convention, κ values are normalized to a standard state by using the surface tension of pure water and room temperature ($\sigma = 0.072$ N m^{-1}, $T = 298.15$ K) in calculations. This κ is denoted as "apparent κ" because it subsumes surface tension and other physicochemical processes to express the observed CCN activation or water uptake. Specifying any two of the variables κ, s_c, D_d or the variables κ, S, G_f will uniquely determine the third, facilitating intercomparison of values across different studies. Hereafter "hygroscopicity" and "κ" refer to apparent κ unless otherwise specified.

Mismatch between κ derived from CCN measurements and κ derived from subsaturated measurements has been observed[35,36] but remains difficult to interpret. Contributing factors include reduced surface tension,[36,37] solubility limitations,[38] and particle irregularity and surface restructuring during measurements.[39] To account for these factors, we further differentiate between apparent κ and intrinsic κ, κ_{intr}, which can be expressed by fully dissolved compounds in the absence of surface tension reduction or particle irregularities during the measurement.[40] For a mixture of compounds of limited solubility, $\kappa = \sum_i \epsilon_i \kappa_{intr,i} H(x_i)$, where ϵ_i is the volume fraction of the ith component in the dry particle, $\kappa_{intr,i}$ is the intrinsic κ of the ith component, and $H(x_i)$ is the dissolved fraction of the solute. This fraction is found using $x_i = C_i V_w / V_{s,i}$, where C_i is the aqueous solubility of the ith component expressed as volume solute per volume water at saturation, V_w is the volume of water, and $V_{s,i}$ is the total dry volume of the ith component. The fraction dissolved is then $H(x_i) = x_i$ for partial dissolution ($x_i < 1$) and $H(x_i) = 1$ for complete dissolution ($x_i \geq 1$). For pure compounds, κ is given by

$$\kappa = H(x)\kappa_{intr} \quad (3)$$

Based on eq 3, for dissolved compounds ($H(x) = 1$), measurements of $\log(s_c)$ as a function of varying $\log(D_d)$ follow κ isolines with a slope of $\sim -3/2$. For compounds with limited solubility ($H(x) < 1$), the measurements will exhibit off-isoline behavior at the onset of solubility limitation, when the particles are not fully dissolved at the point of activation.[34,41−43]

CCN activity was modeled using the open-source U-CCN model of Petters et al.[30] In this study improvements to the UNIFAC core (Fredenslund et al.[26] eqs 1−7 with the parameters table given by Petters et al.[30] containing values from Hansen et al.,[44] Raatikainen and Laaksonen,[28] and Compernolle et al.[29]) are investigated for the hydroperoxide functional group. We specifically seek interaction parameters that are optimal for CCN predictions only. As we have shown previously,[30,45] the transition from CCN inactive ($\kappa \sim 0$) to CCN active (κ consistent with predictions based on molar volume) requires the removal of solubility/miscibility limitations. Thus, the prediction for compounds with solubility limitations is highly sensitive to the water activity and liquid−liquid phase separation prediction at water activities very near unity. Three approaches were taken: (1) original parameters were used ("default approach"); (2) the CH(OOH) subgroup was replaced with a CH(O) and an OH group ("replacement approach");[29,46,47] and (3) the CH(OOH) parameters were adjusted based on an exhaustive grid search ("adjusted approach"). A brute force grid search was performed seeking a new pair of UNIFAC interaction parameters[26] ($a_{m\to n}$, $a_{n\to m}$) for hydroperoxide (m) and water (n). This procedure produced a line in parameter space for which the mean error was ~0. These values are summarized in the Supporting Information. Along this line, SSE asymptotically approached a low value. The variation of modeled apparent κ as a function of carbon chain length showed that some parameters result in unphysical behavior, and these parameters are discarded. Unphysical behavior is diagnosed by plotting simulated homologous series of functionalized n-alkanes.[30] The physical basis for the unphysical regions is that due to its reduced oxidation state, the water affinity of the hydroperoxide group should not exceed that of the hydroxyl group. The primary effects on CCN activity are molecular size and water solubility/miscibility, and secondary effects include activity coefficients and surface tension; thus, the U-CCN model captures the majority of the physical processes. Specifics about the procedure to constrain the parameter space to a physical solution are provided in the

DOI: 10.1021/acs.jpca.7b04114
J. Phys. Chem. A 2017, 121, 5164−5174

Supporting Information. Adjusted parameters were selected from within the set of reasonable parameters based on lowest available mean error and SSE. These parameters are $a_{m\rightarrow n}$ = −667.3 and $a_{n\rightarrow m}$ = 963.6. In discussion to follow, UNIFAC refers to the model with adjusted parameters unless otherwise specified. For the adjusted parameters the sum square error (SSE), $\sum(\log(\kappa_{\mathrm{model}}) - \log(\kappa_{\mathrm{observed}}))^2$, and the mean error, $\mathrm{mean}(\log(\kappa_{\mathrm{model}}) - \log(\kappa_{\mathrm{observed}}))$, were both assessed. The modeled behavior of hypothetical C_6−C_{35} hydroperoxides was evaluated.

CCN activity was also estimated independently based on modeled molar volume and Flory−Huggins−Köhler theory, which assumes an athermal mixture of molecules of different sizes, considering only the entropy of mixing.[48] Because it ignores chemical interactions, Flory−Huggins−Köhler theory describes the CCN activity for compounds that are completely dissolved at compositions corresponding to water contents at the critical supersaturation.[45,49] Flory−Huggins−Köhler theory has been shown to model the CCN activity of effectively soluble molecules with molecular weights ranging from 80 to 2000 Da.[45]

EXPERIMENTAL SECTION

Two types of organic compounds were synthesized for this study: compounds containing hydroperoxy groups and compounds containing carbonyl groups. Hydroperoxides included three isomers each of C_{10}, C_{12}, C_{14}, and C_{16} hydroperoxyacids (alkoxy hydroperoxyalkanoic acids) and the same number of dihydroperoxides (dialkoxy dihydroperoxyalkanes). Carbonyls included a C_{16} dione, C_{18} diketoaldehyde, and a C_{19} ketoester. Hydroperoxides were synthesized in solution by ozonolysis of either an alkenoic acid or diene in the presence of excess alcohol.[50,51] Details of the synthesis are reported in the Supporting Information, and the reaction mechanism is reproduced in Scheme S1. Precursor compounds, targeted molecular structures, molecular weights, molar volumes estimated from the U-CCN model, computer readable SMILES strings (simplified molecular input line-entry system), and UNIFAC representations are summarized in Tables S2 and S3. The alcohols and alkenes were selected to determine the carbon chain length of the hydroperoxide product as well as the placement of the functional groups. A total of 24 hydroperoxides were synthesized.

Synthesized hydroperoxides were purified using reverse-phase high-performance liquid chromatography (HPLC) as described in previous work.[23,25] Compound fractionation was achieved using an Agilent 1100 series HPLC equipped with an Agilent Zorbax Eclipse Plus XDB-C18 column (250 × 4.6 mm, 5 μm particle size) at room temperature and a Zorbax Reliance cartridge guard column (4.6 × 12.5 mm with 5 μm particle size) with a flow rate of 0.8 mL min^{-1}. A gradient elution method was employed starting with a 5:95 acetonitrile:water mixture for 5 min, then ramping to 100:0 over 50 min, and holding at this composition for 15 min. The column eluent was routed directly to a Collison atomizer, where the solution was atomized, passed through silica gel and charcoal diffusion driers to remove the solvent, and residual hydroperoxide particles were routed to the scanning flow-CCN measurement setup described below.

Carbonyls were synthesized and purified using a method we have employed previously[52] and which is described in the Supporting Information. ^{1}H and ^{13}C NMR were used to verify the structure and purity of the synthesized compounds. Molecular structures, SMILES strings, molecular weights, modeled molar volumes from the U-CCN model, and UNIFAC representations are summarized in Table S4. The purified carbonyls were dissolved in acetonitrile, atomized, and dried, and the residual carbonyl particles were then routed to a scanning mobility particle sizer (SMPS)-CCN measurement and a hygroscopicity tandem differential mobility analyzer (HTDMA), both of which are described below.

The CCN measurement setup had two modes of operation: scanning flow-CCN[23,25,53] and SMPS-CCN.[54,55] Schematics of these previously described setups are provided in Figures S1 and S2. Scanning flow-CCN mode had a faster duty cycle and was used to capture eluting HPLC peaks; SMPS-CCN mode had a larger dynamic range and was used for selected dihydroperoxides and for the already-purified carbonyls. In all cases aerosol was size-selected by a differential mobility analyzer (DMA; TSI 3071A) operated at 9:1.5 L min^{-1} sheath-to-sample flow ratio. The flow was split between a condensation particle counter (CPC; TSI 3010, 1 L min^{-1}) and a streamwise gradient continuous flow CCN counter[56] (DMT, 0.5 L min^{-1}). CCN instrument supersaturation was determined using size-selected ammonium sulfate aerosol and the Aerosol Inorganic Model[57,58] to relate dry diameter and critical supersaturation.[25,41,59] For scanning flow-CCN measurements, the diameter was held constant while the CCN flow was scanned linearly from ∼0.3 to 1.0 L min^{-1} in 44 s, translating to a supersaturation scan of 0.2−1.1%. For SMPS-CCN measurements the DMA voltage was exponentially ramped from 9000 to 50 V in 220 s, translating to a diameter ramp from 330 to 20 nm.[55,60] SMPS-CCN data were inverted to correct for multiply charged particles as described previously.[61] Supersaturation and diameter at 50% activation were used to calculate apparent κ using eq 1.

The HTDMA instrument has been described previously[62−64] and measured the humidified diameter of wet aerosols at a controlled relative humidity.[65] A schematic of the setup is provided in Figure S3. Dry 100 nm particles were selected by a DMA (TSI 3080) before humidification by passage through a Nafion membrane immersed in water. The water temperature dictates the dewpoint of the sample,[66] which is then passed to a thermally isolated high-flow DMA[67] whose temperature inhomogeneities are actively held within ±0.02 °C.[62] The instrument was operated in comparative hygroscopicity mode. In this mode the aerosol flow to the instrument alternates between sample aerosol and ammonium sulfate. The ammonium sulfate growth factor is used to determine the relative humidity inside the instrument.[62−64] Two important modifications were made to the HTDMA instrument. First, the high flow DMA was placed in a secondary temperature controlled enclosure that was held at ∼19 °C, in addition to the heat exchangers mounted to the column.[62] The slight cooling below room temperature (22−30 °C) allowed for stable long-term humidification at a relative humidity of 99% while avoiding condensation of vapor in lines outside the secondary enclosure. Second, the humidified size distributions were characterized using 10 Hz data acquisition, scanning from 3000 to 50 V in 50 s using a sheath:sample flow ratio of 14.5:1. The fast scans were implemented to interface the instrument with the HPLC system (data not shown here). The rapid scanning leads to smearing of the peak. However, it was verified experimentally that the accuracy of the retrieved mode diameter was not affected by the scan rate. Because of limited instrument availability, only carbonyls were measured using the HTDMA

DOI: 10.1021/acs.jpca.7b04114
J. Phys. Chem. A 2017, 121, 5164−5174

instrument. Relative humidities and growth factors were used to calculate apparent κ using eq 2.

RESULTS AND DISCUSSION

Figure 1 and Table S5 summarize results for the hygroscopicity of hydroperoxyacids. Hygroscopicity decreased with increasing

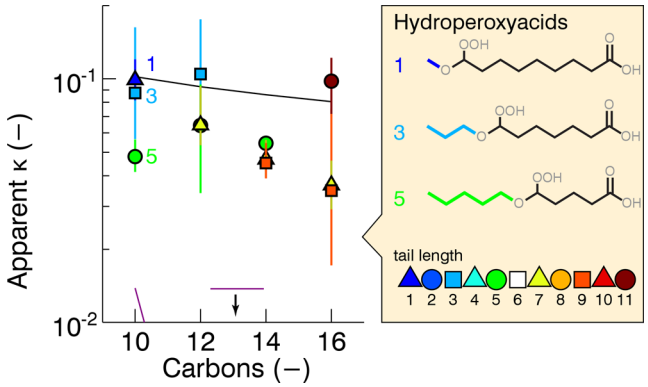

Figure 1. Hygroscopicity of hydroperoxyacids (alkoxy-hydroperoxyalkanoic acids) as a function of carbon chain length. Selected molecules are pictured at right. Each point is the average of several experiments, and error bars indicate the minimum and maximum of all results. Colors indicate the length of the hydrophobic alkyl tail. The black line shows the Flory–Huggins prediction, and the purple line shows the adjusted approach U-CCN model prediction. For $C_n \geq C_{11}$, the U-CCN prediction is below the lower limit of the ordinate.

carbon chain length and ranged from κ = 0.1 to 0.03. The data fall between the Flory–Huggins prediction, which overpredicted κ for some but not all of the isomers, and the adjusted U-CCN model prediction, which greatly underpredicted κ. This underprediction is discussed below in the context of the U-CCN model adjustment. Molecules with the hydroperoxy group near the end of the carbon chain tend to have larger κ and were predicted better by Flory–Huggins–Köhler theory. Compounds that fall below the Flory–Huggins prediction undergo solubility (referring to solubility of crystalline solids) or miscibility (referring to liquid–liquid phase separation) controlled droplet activation and are expected to be only sparingly soluble/miscible in water.

Figure 2 and Table S6 summarize the hygroscopicity measurements of the dihydroperoxides. Hygroscopicity decreased with increasing carbon chain length and ranged from κ = 0.05 to 0.007. The rate of decrease is more rapid and reaches lower values than for the hydroperoxyacids. All data fell below the Flory–Huggins prediction, suggesting that the dihydroperoxides are sparingly soluble in water. The data are reasonably well described by the adjusted U-CCN model prediction, although several isomers have κ values that are significantly lower than the adjusted U-CCN model. With the exception of C_{10} compounds, the dihydroperoxides with the COOH group positioned closer to the center of the molecule were more hygroscopic, consistent with our previous results for similar dihydroperoxides.[23]

Although at present the observed isomeric differences evident in the data in Figures 1 and 2 are within the uncertainty of the HPLC-CCN technique (i.e., the error bars overlap), it is known that the position of organic functional groups can affect compound properties including the hygroscopicity,[68] solubility,[69] vapor pressure,[70,71] melting point,[72,73] reaction mechanisms,[74−76] viscosity,[77] and glass-

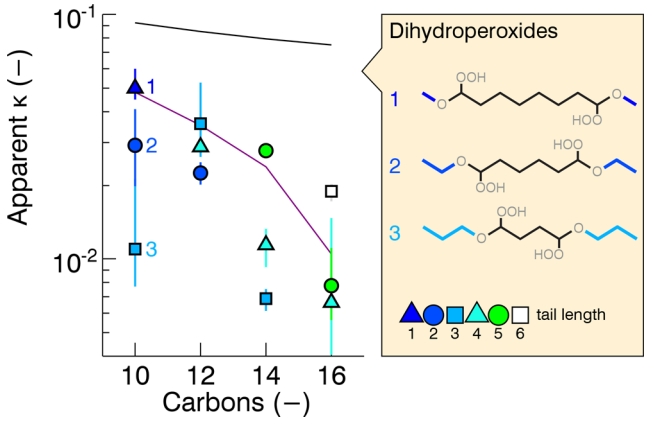

Figure 2. Hygroscopicity of dihydroperoxides (dialkoxy-dihydroperoxyalkanes) as a function of carbon chain length. Each point is the average of several experiments, and error bars indicate the minimum and maximum of all results. Colors indicate the length of the hydrophobic alkyl tail. The black line shows the Flory–Huggins prediction, and the purple line shows the adjusted approach U-CCN model prediction.

transition temperatures.[78] The behavior of dihydroperoxides is broadly consistent with the hypothesis that polar functional groups are more efficient in promoting solubility if they are positioned near the center of the molecule.[69] The hydroperoxyacids do not show a strong correlation between the length of the hydrophobic alkyl tail and isomer hygroscopicity. Competing effects may be at play. The hydrophobic tail may fold as solvating water molecules attract polar functional groups to the solvation shell of the molecule, and since folded isomers tend to have a reduced effective molecular size,[69] they may be more hygroscopic.[45,49] However, if the tail instead forms a hydrophobic branch, it may disrupt the first solvation layer of water molecules, reducing hygroscopicity. These effects are influenced by the specific geometries of molecules, and standard UNIFAC is indifferent toward the location of functional groups. Therefore, isomer effects cannot be resolved with the U-CCN model. Marcolli and Peter[68] modified the UNIFAC functional group definitions to separately account for molecular alkyl tails, and although this approach is attractive, caveats include the need for more fitted parameters and the absence of a large volume of observational data.

Figure 3 and Table S7 summarize the additional tests of hygroscopicity and supersaturation at CCN activation of C_{10} and C_{12} dihydroperoxides as a function of particle dry diameter. Specifically, isomers #2.1 and #2.4 (Table S3) are shown (the C_{10} square and C_{12} triangle in Figure 2). Each isomer was measured twice, and differences between the first and the repeated experiments are consistent with the ±10% variability in the supersaturation of the CCN instrument. The relationship between critical supersaturation and dry diameter shows an inflection point (panels A and C) where the C_{10} dihydroperoxide observation departs from the κ isoline. No inflection point is observed for the C_{12} dihydroperoxide. The off-isoline behavior is usually attributed to sparing solubility of the compound.[34,41−43] The pure-compound κ model including solubility[34] (eq 3) describes the observations well in both cases. Based on the best fit of eq 3 to the data, the solubility of the C_{10} compound was C = 0.31 with κ_{intr} = 0.042 and the solubility of the C_{12} compound was C = 0.52 with κ_{intr} = 0.04. The solubility-controlled transition in apparent κ (i.e., the inflection

DOI: 10.1021/acs.jpca.7b04114
J. Phys. Chem. A 2017, 121, 5164−5174

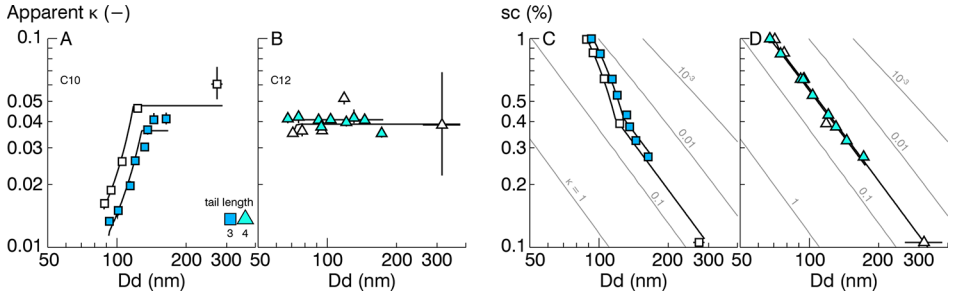

Figure 3. Hygroscopicity of dihydroperoxides as a function of particle dry diameter (A, B) and supersaturation at activation as a function of particle dry diameter (C, D). Panels A and C show the C_{10} dihydroperoxide (tail length 3), and panels B and D show the C_{12} dihydroperoxide (tail length 4). Open symbols indicate a repeated experiment. Each point is the average of ~3 experiments. Error bars indicate the range of measured values. Gray lines of constant hygroscopicity are shown in panels C and D. Black lines show the κ solubility model for pure compounds (eq 3).[34]

point) began for C_{10} dihydroperoxide particles near D_d = 150 nm (panel A). The C_{10} particles were not fully dissolved at the point of activation for D_d < 150 nm due to their solubility. The undissolved fraction increased at lower diameters and could not contribute water uptake to the growing droplet. The C_{12} compounds did not exhibit significant solubility limitations in the range measured.

The success of the pure-compound κ solubility framework in describing the observations in Figure 3 is consistent with the near unity yields expected for the target hydroperoxides produced in the synthesis of these standards.[50,79−81] It is reassuring that these compounds behave as pure compounds, given that for this set of solubility experiments the HPLC purification step was skipped (due to its very low throughput). The HPLC-CCN measurements of the C_{10} dihydroperoxide isomers in Figure 2 were collected in a diameter range (123, 123, and 177 nm; Table S6) close to the onset of solubility limitations shown in Figure 3 (panel A). Thus, it is unsurprising that their apparent κ = 0.011 fell short of the fitted κ_{intr} = 0.042 in Figure 3. The C_{12} dihydroperoxide apparent κ = 0.029 was nearer the fitted κ_{intr} = 0.04. Many sparingly soluble compounds that should show inflection points do not in practice.[34,42,43,82,83] Reasons for this behavior frequently cited in the literature are solubilization of the analyte by trace impurities present in the particle and uncertainties about the dried particle phase state.[42,82]

We now explore if effects other than solubility, such as reduced surface tension, viscosity, or volatility, could contribute to the observed CCN data. Solubility, surface tension reduction, viscosity, volatility, and hygroscopicity are all linked to molecular structure. The surface tension of C_{12} and C_{10} dihydroperoxides in aqueous solution is expected to lie between that of sodium fatty acid salts and dicarboxylic acids (cf. Figure 1 of Petters and Petters[55]), based on functional group composition and carbon chain length. Thus, the surface tension reduction may affect CCN activation. However, Figure 3A shows a sharp reduction in κ at smaller diameters, contrary to model predictions that show larger κ at smaller diameters regardless of the extent to which the surfactant partitions to the surface.[36,55,84] Facchini et al.[85] proposed that surface tension reduction during CCN activation greatly enhances the CCN activity of organic compounds. This prediction was made using bulk measurements of surface tension from environmental samples. Bulk measurements have also been used to predict strong CCN enhancement in more recent work (e.g., Giordano et al.[86] and Nozière et al.[87]). The problem with this approach is that hygroscopic growth and CCN activation are controlled by both surface tension and water activity, and the partitioning of surfactants to the surface of small droplets perturbs the water activity within the droplet.[88−90] Measurements of CCN activity for surfactant compounds have repeatedly shown that strong CCN enhancement does not occur,[55,90,91] and delayed CCN activation tests show that the partitioning of surfactants is likely not time dependent within the measurement time scale.[92] Measurement of surface tension is typically done in the bulk. Although measurements have been recently extended to sizes as small as 5 μm, this is still much larger than the growing and activating CCN droplet.[93] The surface tension of droplets is undoubtedly perturbed by the solute; however, few authors are willing to attribute their discrepancies entirely to surface tension reduction.[36,37] Several theories predicting surface partitioning in nanoscale droplets have been developed[89,94−96] and may be included in future versions of the U-CCN model.

Based on the molecular structures, the viscosities of the compounds in this study are well below the 100 Pa·s delineation between liquid and semisolid,[97] making it unlikely that water uptake was kinetically limited by water diffusion through the condensed phase organic matrix. It is surprising, however, that the C_{10} compound exhibited a lower solubility than the C_{12} compound because the larger molecule would be expected to be less soluble due to the addition of the hydrophobic group. One potential explanation is volatility. If the C_{10} particles partially evaporated in the CCN instrument, a lower κ would be measured. The thermal gradient in the CCN instrument is larger for larger supersaturation, and thus the decrease in κ with increasing supersaturation might be also due to volatilization.[98] Volatilization experiments that measure aerosol diameter changes at ambient[99,100] or chilled temperatures[64] or with liquid water to inhibit evaporation[60,101,102] could probe this hypothesis.

Figure 4 shows the hygroscopicity of C_{14} hydroperoxide compounds as a function of the number of carboxyl (panel A) or hydroperoxy (panel B) groups. Hygroscopicity increased with the number of functional groups, consistent with previous results.[23] Hydroperoxyacids measured here (panel A) were slightly more CCN active ($\kappa \sim 0.05$) than previous results ($\kappa \sim 0.02$) but lie within the experimental uncertainty shown in Figure 1. Note that only the isomer with a C_5 tail was measured in both studies. The observed slope $d(\kappa)/d(\text{carboxyl})$ was roughly equivalent to the slope of the adjusted U-CCN model prediction. Current dihydroperoxide (panel B) observations are consistent with previous results and range from κ = 0.007 to 0.03. The observed slope $d(\kappa)/d(\text{hydroperoxy})$ was shallower than the U-CCN model prediction. The U-CCN prediction of κ was consistent with observations for dihydroperoxides but underpredicted κ for the hydroperoxyacids and monofunctional

DOI: 10.1021/acs.jpca.7b04114
J. Phys. Chem. A 2017, 121, 5164−5174

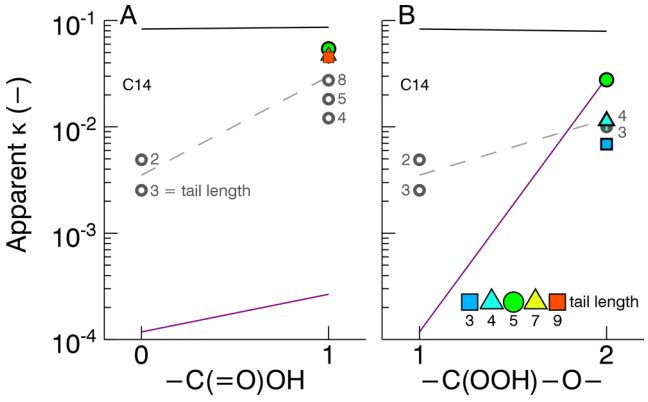

Figure 4. Hygroscopicity of C_{14} hydroperoxides as a function of the number of carboxyl (A) and hydroperoxy (B) groups. Data from Suda et al.[23] are included for comparison (open circles). Each point is the average of several experiments and error bars indicate range. The length of the hydrophobic alkyl tail is indicated with a number (Suda et al.[23]) or a color (this work). The black line shows the Flory–Huggins prediction, the dotted gray line shows the observed slope, and the purple line shows the adjusted U-CCN model.

hydroperoxides. All compounds were less CCN active than the Flory–Huggins model prediction.

Figure 5 and Table S8 summarize the hygroscopicity of carbonyls as a function of carbon chain length. Hygroscopicity

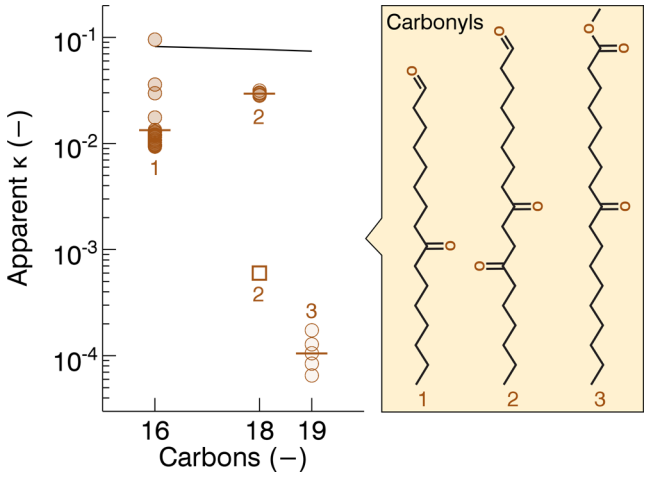

Figure 5. Hygroscopicity of carbonyls as a function of carbon chain length. All compounds are pictured at right. Averages (horizontal lines) and individual measurements (circles) are both shown. Subsaturated measurements (using HTDMA technique) are shown if they were above the detection limit (square). The black line shows the Flory–Huggins prediction. The U-CCN model prediction was $\kappa \sim 0$.

ranged from 0.0001 to 0.03, generally decreasing with carbon number and increasing with the number of keto groups. Between compounds 1 and 2, the addition of a keto group raises κ despite the addition of two carbons. Between compounds 2 and 3, the loss of a keto group renders compound 3 effectively CCN inactive. All observations fall below the Flory–Huggins prediction, likely due to solubility limitations. The U-CCN model prediction was $\kappa \sim 0$. Nevertheless, the increase in κ between compounds 1 and 2 shows that the keto group promotes CCN activity. This trend is qualitatively consistent with predictions for carbonyls of lower molar mass.[30]

Figure 5 also shows HTDMA measurements of carbonyl compounds (summarized in Table S9). The diameter growth factor, G_f from eq 2, was 0.809, 1.007, and 0.877 for carbonyl compounds 1, 2, and 3 at 98–99% relative humidity. The C_{18} diketoaldehyde showed significantly lower κ for measurements taken at subsaturated relative humidity than for those taken at supersaturated relative humidity. Growth factors less than 1 could be indicative of slight evaporation or surface restructuring upon humidification.[39,103] The growth factor of the C_{18} diketoaldehyde corresponds to $\kappa = 0.0006$ at 98.7% relative humidity; compounds with negative κ are not included because water uptake was below the detection limit.

Figure 6 shows the relationship between the measured and modeled CCN activity for hydroperoxides using the three different model approaches. The underprediction of κ using the default approach is a prominent feature (panel A). The C_{12} hydroperoxyacids (all isomers; labeled "2") and C_{10} dihydroperoxides (all isomers; labeled "5") have larger error because some of the diameters corresponded to sizes where κ varies strongly due to miscibility limitations. In panel B, the replacement approach performed well for the dihydroperoxides (green circles 5–8 and purple square 12) and underpredicted κ for other compounds (hydroperoxyacids and C_{14} hydroperoxides from previous work).[23,30]

Predictions for the adjusted approach are superimposed in Figures 1, 2, and 4. These figures show that the U-CCN model captured the absolute κ value and the relationship between κ and carbon number well for the dihydroperoxides (Figure 2). In contrast, predictions are poor for the hydroperoxyacids (Figure 1) and C_{14} monofunctional hydroperoxides (Figure 4). Figure 6 panels C and D summarize the same data. The adjusted approach performed slightly better than the replacement approach. The observed ranges in κ were generally larger than the modeled ranges likely in part due to the different isomers measured, which UNIFAC cannot distinguish.

The closeness between the Flory–Huggins prediction and the data (Figure 1) suggests that the hydroperoxyacids were sufficiently soluble, i.e., that the $H(x)$ term in eq 3 approaches unity. This is clearly not captured by U-CCN model for this specific functional group pair. Potential explanations for this behavior include strongly reduced surface tension, presence of trace impurities, interactions between the hydroperoxide and acid groups that render the molecule soluble but are not captured in the functional group framework, or acid–water group interaction parameters that are not tuned well enough to exactly model miscibility/solubility. At this time the data generated for this work and the compounds analyzed in previous work[23] are insufficient to conclusively attribute the source of the error. Additional CCN studies targeting the carboxyl group will be needed.

The gray regions in Figure 6 show κ values that are too low to be considered CCN active under typical warm cloud (e.g., stratus) conditions. Compounds in these regions do not participate in water uptake and contribute to CCN activity only by virtue of the effect of their dry volumes on the overall diameter of a growing droplet. As compounds evolve by photochemical oxidation in the atmosphere, they generally become more hygroscopic,[15,16] leaving the CCN-inactive region of Figure 6. This solubility-controlled transition is aided by the addition of hygroscopic functional groups to the carbon backbone[23] and will be better estimated as more

DOI: 10.1021/acs.jpca.7b04114
J. Phys. Chem. A 2017, 121, 5164–5174

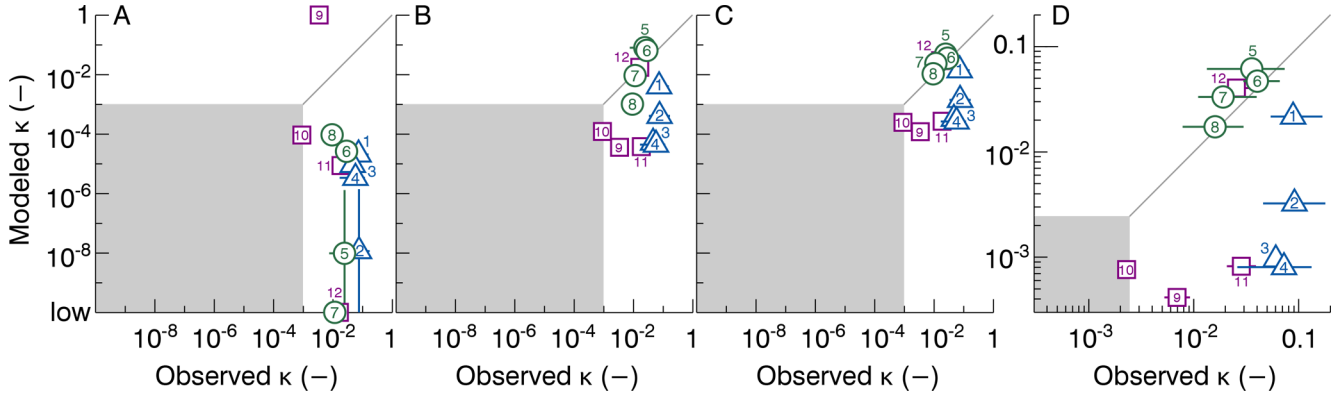

Figure 6. Hydroperoxide hygroscopicity modeled by the U-CCN model as compared with the observed hygroscopicity. Panel A shows the default approach; panel B shows the replacement approach; and panels C and D show the adjusted approach. Panel D uses different axis scaling. Error bars indicate the range of observed values for different isomers (*x*-error) and the range of modeled values for different dry diameters (*y*-error). Gray shading indicates where compounds are inactive as CCN under typical stratus conditions. Blue triangles numbered 1−4 refer to C_{10}, C_{12}, C_{14}, and C_{16} hydroperoxyacids (Tables S2 and S5); green circles numbered 5−8 refer to C_{10}, C_{12}, C_{14}, and C_{16} dihydroperoxides (Tables S3 and S6); and purple squares numbered 9−12 refer to C_{14} hydroperoxides from previous work.[23,30]

hygroscopicity measurements for different functional groups become available.

To our knowledge, this and our previous work[23] constitute the first measurements of the CCN activity of pure organic hydroperoxides available in the literature. Compernolle et al.[29] derived hydroperoxide interaction parameters based on the SPARC (Sparc Performs Automated Reasoning in Chemistry)[104] model. These parameters have since been implemented in several UNIFAC models that predict water uptake.[30,47] Why does SPARC underpredict interactions between hydroperoxides and water? The Compernolle parameters were intended for use in predicting vapor−liquid equilibrium of α-pinene reaction products, and the authors point out that as water uptake increases, the accuracy of these interaction parameters for UNIFAC will decrease because hydroperoxides participate in hydrogen bonding. The ability of polar organics to form associated solutions or to be solvated by water generally complicates their treatment in models. Multifunctional hydroperoxides are known to form intra- and intermolecular hydrogen bonds.[48,105−107] For example, hydrogen bonding can draw the molecules closer together or contract them, leading to misestimated molar volume in solutions.[32,108,109] Similarly, hydroperoxides can form dimers or larger clusters via hydrogen bonds,[48,106,107] thereby acting as larger molecules in solution.[48] These complex interactions may contribute to the difficulty of uniquely representing hydroperoxides within the UNIFAC modeling framework. Petters et al.[30] used the U-CCN model with homologous series to quantify how effective functional groups are in removing solubility limitations to CCN activation. These sensitivities can be expressed by comparison to effect of changing carbon chain length (CH_n). For example, to maintain constant CCN activity, one hydroxyl group (promoting solubility) compensates for the addition of four CH_n groups (reducing solubility), and this is expressed as $\Delta[CH_n]/\Delta[OH] \sim -4$. The sensitivity for the hydroperoxy group using the U-CCN model default approach is $\Delta[CH_n]/\Delta[CH_n(OOH)] \sim -2$. Conversely, the sensitivity for the hydroperoxy group using the adjusted approach is $\Delta[CH_n(OOH)]/\Delta[CH_n] \sim -4$, similar to that of a hydroxyl group. This is physically reasonable given that both functional groups form hydrogen bonds with water molecules.

CONCLUSIONS

Twenty-seven compounds were synthesized to systematically investigate how the number and location of functional groups affect CCN activity. Measurements of CCN activity were performed for three main compound groups: alkoxyhydroperoxyalkanoic acids (hydroperoxyacids), dialkoxydihydroperoxyalkanes (dihydroperoxides), and carbonyls. For most compounds the sample was purified with HPLC, and the HPLC eluent was interfaced with scanning flow-CCN analysis to determine the CCN activity expressed as an apparent κ value.

Hydroperoxyacids were more CCN active than dihydroperoxides of the same carbon chain length. The keto functional group promoted CCN activity. CCN activity generally decreased with increasing carbon chain length. Polar functional groups closer to the center of the molecule were more effective in promoting CCN activity except for the hydroperoxyacids that did not show this pattern. This may be due to folding of the hydrophobic alkane tail of the molecules, which can simultaneously reduce molecular size (promoting hygroscopicity) and disrupt the first solvation layer of water (reducing hygroscopicity).

Size and supersaturation-resolved CCN experiments were performed with two dihydroperoxide compounds and showed that solubility limitations were likely responsible for measured CCN activity below the Flory−Huggins prediction from molecular size. The C_{10} dihydroperoxide appeared to have limited solubility at CCN activation for dry diameters less than 150 nm, while the C_{12} dihydroperoxide did not.

The data collected in this work were used to evaluate the performance of a group contribution model that predicts CCN activity. This model combines a UNIFAC core, a molar volume prediction, and a liquid−liquid phase separation algorithm with Köhler theory to model the activation diameter for organic compounds. Improved hydroperoxide−water group interaction parameters were derived. The adjusted parameters result in excellent agreement between the data and the dihydroperoxide compounds. However, the adjusted parameter model still underestimates CCN activity for the monfunctional hydroperoxides and hydroperoxyacids. Potential explanations for this behavior include strongly reduced surface tension, trace impurities that remove solubility or miscibility limitations,

DOI: 10.1021/acs.jpca.7b04114
J. Phys. Chem. A 2017, 121, 5164−5174

hydroperoxide−acid group interactions that promote solubility but are not captured in the functional group framework, or acid−water group interaction parameters that do not capture miscibility/solubility near the point of droplet activation. Additional studies are required to better understand the cause of these discrepancies. The net result of the adjusted parameters is that the hydroperoxide group is approximately as effective as the hydroxyl group in removing solubility/miscibility limitations from otherwise nonpolar molecules. This similarity between OH and $CH_n(OOH)$ is unsurprising due to the expected underlying hydrogen bonding driving solvation and dissolution processes of the molecule.

■ ASSOCIATED CONTENT

Supporting Information

The Supporting Information is available free of charge on the ACS Publications website at DOI: 10.1021/acs.jpca.7b04114.

Synthesis of compounds; instrument schematics; synthesized compounds, experimental results, and modeling results; and exhaustive grid search for adjusted parameters (PDF)

■ AUTHOR INFORMATION

Corresponding Author

*(S.S.P.) E-mail spetters@unc.edu.

ORCID

Sarah Suda Petters: 0000-0002-4501-7127

Markus D. Petters: 0000-0002-4082-1693

Paul J. Ziemann: 0000-0001-7419-0044

Present Address

S.S.P.: Department of Environmental Sciences and Engineering, University of North Carolina at Chapel Hill, Chapel Hill, NC 27599-7400.

Notes

The authors declare no competing financial interest.

■ ACKNOWLEDGMENTS

This research was funded by the United States Department of Energy, Office of Science, Grant DE-SC 0012043. The authors thank Patrick Chuang for the use of the high flow DMA and Timothy Wright for construction of the HTDMA enclosure and high-resolution scanning software.

■ REFERENCES

(1) Köhler, H. The nucleus in and the growth of hygroscopic droplets. *Trans. Faraday Soc.* **1936**, *32*, 1152−1161.

(2) Farmer, D. K.; Cappa, C. D.; Kreidenweis, S. M. Atmospheric processes and their controlling influence on cloud condensation nuclei activity. *Chem. Rev.* **2015**, *115* (10), 4199−4217.

(3) Ångström, A. On the atmospheric transmission of sun radiation and on dust in the air. *Geografiska Annaler* **1929**, *11*, 156−166.

(4) Yu, H.; Kaufman, Y. J.; Chin, M.; Feingold, G.; Remer, L. A.; Anderson, T. L.; Balkanski, Y.; Bellouin, N.; Boucher, O.; Christopher, S. A.; et al. A review of measurement-based assessments of the aerosol direct radiative effect and forcing. *Atmos. Chem. Phys.* **2006**, *6* (3), 613−666.

(5) Dockery, D. W.; Pope, C. A.; Xu, X.; Spengler, J. D.; Ware, J. H.; Fay, M. E.; Ferris, B. G.; Speizer, F. E. An association between air pollution and mortality in six U.S. Cities. *N. Engl. J. Med.* **1993**, *329* (24), 1753−1759.

(6) West, J. J.; Cohen, A.; Dentener, F.; Brunekreef, B.; Zhu, T.; Armstrong, B.; Bell, M. L.; Brauer, M.; Carmichael, G.; Costa, D. L.; et al. What we breathe impacts our health: Improving understanding of the link between air pollution and health. *Environ. Sci. Technol.* **2016**, *50* (10), 4895−4904.

(7) Zhang, Q.; Jimenez, J. L.; Canagaratna, M. R.; Allan, J. D.; Coe, H.; Ulbrich, I.; Alfarra, M. R.; Takami, A.; Middlebrook, A. M.; Sun, Y. L.; et al. Ubiquity and dominance of oxygenated species in organic aerosols in anthropogenically-influenced northern hemisphere midlatitudes. *Geophys. Res. Lett.* **2007**, *34* (13), L13801.

(8) Goldstein, A. H.; Galbally, I. E. Known and unexplored organic constituents in the earth's atmosphere. *Environ. Sci. Technol.* **2007**, *41* (5), 1514−1521.

(9) Kroll, J. H.; Seinfeld, J. H. Chemistry of secondary organic aerosol: Formation and evolution of low-volatility organics in the atmosphere. *Atmos. Environ.* **2008**, *42* (16), 3593−3624.

(10) Ziemann, P. J.; Atkinson, R. Kinetics, products, and mechanisms of secondary organic aerosol formation. *Chem. Soc. Rev.* **2012**, *41* (19), 6582−6605.

(11) Blando, J. D.; Turpin, B. J. Secondary organic aerosol formation in cloud and fog droplets: A literature evaluation of plausibility. *Atmos. Environ.* **2000**, *34* (10), 1623−1632.

(12) Carlton, A. G.; Turpin, B. J.; Altieri, K. E.; Seitzinger, S. P.; Mathur, R.; Roselle, S. J.; Weber, R. J. CMAQ model performance enhanced when in-cloud secondary organic aerosol is included: Comparisons of organic carbon predictions with measurements. *Environ. Sci. Technol.* **2008**, *42* (23), 8798−8802.

(13) Ervens, B.; Turpin, B. J.; Weber, R. J. Secondary organic aerosol formation in cloud droplets and aqueous particles (aqSOA): A review of laboratory, field and model studies. *Atmos. Chem. Phys.* **2011**, *11* (21), 11069−11102.

(14) McNeill, V. F. Aqueous organic chemistry in the atmosphere: Sources and chemical processing of organic aerosols. *Environ. Sci. Technol.* **2015**, *49* (3), 1237−1244.

(15) Jimenez, J. L.; Canagaratna, M. R.; Donahue, N. M.; Prévôt, A. S. H.; Zhang, Q.; Kroll, J. H.; DeCarlo, P. F.; Allan, J. D.; Coe, H.; Ng, N. L.; et al. Evolution of organic aerosols in the atmosphere. *Science* **2009**, *326* (5959), 1525−1529.

(16) Chang, R. Y.-W.; Slowik, J. G.; Shantz, N. C.; Vlasenko, A.; Liggio, J.; Sjostedt, S. J.; Leaitch, W. R.; Abbatt, J. P. D. The hygroscopicity parameter (κ) of ambient organic aerosol at a field site subject to biogenic and anthropogenic influences: Relationship to degree of aerosol oxidation. *Atmos. Chem. Phys.* **2010**, *10* (11), 5047−5064.

(17) Mei, F.; Setyan, A.; Zhang, Q.; Wang, J. CCN activity of organic aerosols observed downwind of urban emissions during CARES. *Atmos. Chem. Phys.* **2013**, *13* (24), 12155−12169.

(18) Heald, C. L.; Kroll, J. H.; Jimenez, J. L.; Docherty, K. S.; DeCarlo, P. F.; Aiken, A. C.; Chen, Q.; Martin, S. T.; Farmer, D. K.; Artaxo, P. A simplified description of the evolution of organic aerosol composition in the atmosphere. *Geophys. Res. Lett.* **2010**, *37* (8), L08803.

(19) Kroll, J. H.; Donahue, N. M.; Jimenez, J. L.; Kessler, S. H.; Canagaratna, M. R.; Wilson, K. R.; Altieri, K. E.; Mazzoleni, L. R.; Wozniak, A. S.; Bluhm, H.; et al. Carbon oxidation state as a metric for describing the chemistry of atmospheric organic aerosol. *Nat. Chem.* **2011**, *3* (2), 133−139.

(20) Lambe, A. T.; Onasch, T. B.; Massoli, P.; Croasdale, D. R.; Wright, J. P.; Ahern, A. T.; Williams, L. R.; Worsnop, D. R.; Brune, W. H.; Davidovits, P. Laboratory studies of the chemical composition and cloud condensation nuclei (CCN) activity of secondary organic aerosol (SOA) and oxidized primary organic aerosol (OPOA). *Atmos. Chem. Phys.* **2011**, *11* (17), 8913−8928.

(21) Zhang, F.; Li, Z.; Li, Y.; Sun, Y.; Wang, Z.; Li, P.; Sun, L.; Wang, P.; Cribb, M.; Zhao, C.; et al. Impacts of organic aerosols and its oxidation level on CCN activity from measurement at a suburban site in China. *Atmos. Chem. Phys.* **2016**, *16* (8), 5413−5425.

(22) Rickards, A. M. J.; Miles, R. E. H.; Davies, J. F.; Marshall, F. H.; Reid, J. P. Measurements of the sensitivity of aerosol hygroscopicity and the κ parameter to the O/C ratio. *J. Phys. Chem. A* **2013**, *117* (51), 14120−14131.

DOI: 10.1021/acs.jpca.7b04114
J. Phys. Chem. A 2017, 121, 5164−5174

(23) Suda, S. R.; Petters, M. D.; Yeh, G. K.; Strollo, C.; Matsunaga, A.; Faulhaber, A.; Ziemann, P. J.; Prenni, A. J.; Carrico, C. M.; Sullivan, R. C.; et al. Influence of functional groups on organic aerosol cloud condensation nucleus activity. *Environ. Sci. Technol.* **2014**, *48* (17), 10182−10190.
(24) Petters, M. D.; Kreidenweis, S. M. A single parameter representation of hygroscopic growth and cloud condensation nucleus activity. *Atmos. Chem. Phys.* **2007**, *7* (8), 1961−1971.
(25) Suda, S. R.; Petters, M. D.; Matsunaga, A.; Sullivan, R. C.; Ziemann, P. J.; Kreidenweis, S. M. Hygroscopicity frequency distributions of secondary organic aerosols. *J. Geophys. Res.* **2012**, *117*, D04207.
(26) Fredenslund, A.; Jones, R. L.; Prausnitz, J. M. Group-contribution estimation of activity coefficients in nonideal liquid mixtures. *AIChE J.* **1975**, *21* (6), 1086−1099.
(27) Ming, Y.; Russell, L. M. Thermodynamic equilibrium of organic-electrolyte mixtures in aerosol particles. *AIChE J.* **2002**, *48* (6), 1331−1348.
(28) Raatikainen, T.; Laaksonen, A. Application of several activity coefficient models to water-organic-electrolyte aerosols of atmospheric interest. *Atmos. Chem. Phys.* **2005**, *5* (9), 2475−2495.
(29) Compernolle, S.; Ceulemans, K.; Müller, J.-F. Influence of non-ideality on condensation to aerosol. *Atmos. Chem. Phys.* **2009**, *9* (4), 1325−1337.
(30) Petters, M. D.; Kreidenweis, S. M.; Ziemann, P. J. Prediction of cloud condensation nuclei activity for organic compounds using functional group contribution methods. *Geosci. Model Dev.* **2016**, *9* (1), 111−124.
(31) Zuend, A.; Marcolli, C.; Luo, B. P.; Peter, T. A thermodynamic model of mixed organic-inorganic aerosols to predict activity coefficients. *Atmos. Chem. Phys.* **2008**, *8* (16), 4559−4593.
(32) Girolami, G. S. A simple "back of the envelope" method for estimating the densities and molecular volumes of liquids and solids. *J. Chem. Educ.* **1994**, *71* (11), 962−964.
(33) Eubank, P. T.; Elhassan, A. E.; Barrufet, M. A.; Whiting, W. B. Area method for prediction of fluid-phase equilibria. *Ind. Eng. Chem. Res.* **1992**, *31* (3), 942−949.
(34) Petters, M. D.; Kreidenweis, S. M. A single parameter representation of hygroscopic growth and cloud condensation nucleus activity - Part 2: Including solubility. *Atmos. Chem. Phys.* **2008**, *8* (20), 6273−6279.
(35) Prenni, A. J.; Petters, M. D.; Kreidenweis, S. M.; DeMott, P. J.; Ziemann, P. J. Cloud droplet activation of secondary organic aerosol. *J. Geophys. Res.* **2007**, *112*, D10223.
(36) Irwin, M.; Good, N.; Crosier, J.; Choularton, T. W.; McFiggans, G. Reconciliation of measurements of hygroscopic growth and critical supersaturation of aerosol particles in central Germany. *Atmos. Chem. Phys.* **2010**, *10* (23), 11737−11752.
(37) Wex, H.; Petters, M. D.; Carrico, C. M.; Hallbauer, E.; Massling, A.; McMeeking, G. R.; Poulain, L.; Wu, Z.; Kreidenweis, S. M.; Stratmann, F. Towards closing the gap between hygroscopic growth and activation for secondary organic aerosol: Part 1 - Evidence from measurements. *Atmos. Chem. Phys.* **2009**, *9* (12), 3987−3997.
(38) Petters, M. D.; Wex, H.; Carrico, C. M.; Hallbauer, E.; Massling, A.; McMeeking, G. R.; Poulain, L.; Wu, Z.; Kreidenweis, S. M.; Stratmann, F. Towards closing the gap between hygroscopic growth and activation for secondary organic aerosol − Part 2: Theoretical approaches. *Atmos. Chem. Phys.* **2009**, *9* (12), 3999−4009.
(39) Mikhailov, E.; Vlasenko, S.; Martin, S. T.; Koop, T.; Pöschl, U. Amorphous and crystalline aerosol particles interacting with water vapor: Conceptual framework and experimental evidence for restructuring, phase transitions and kinetic limitations. *Atmos. Chem. Phys.* **2009**, *9* (24), 9491−9522.
(40) Sullivan, R. C.; Moore, M. J. K.; Petters, M. D.; Kreidenweis, S. M.; Roberts, G. C.; Prather, K. A. Effect of chemical mixing state on the hygroscopicity and cloud nucleation properties of calcium mineral dust particles. *Atmos. Chem. Phys.* **2009**, *9* (10), 3303−3316.
(41) Christensen, S. I.; Petters, M. D. The role of temperature in cloud droplet activation. *J. Phys. Chem. A* **2012**, *116* (39), 9706−9717.
(42) Hori, M.; Ohta, S.; Murao, N.; Yamagata, S. Activation capability of water soluble organic substances as CCN. *J. Aerosol Sci.* **2003**, *34* (4), 419−448.
(43) Hings, S. S.; Wrobel, W. C.; Cross, E. S.; Worsnop, D. R.; Davidovits, P.; Onasch, T. B. CCN activation experiments with adipic acid: Effect of particle phase and adipic acid coatings on soluble and insoluble particles. *Atmos. Chem. Phys.* **2008**, *8* (14), 3735−3748.
(44) Hansen, H. K.; Rasmussen, P.; Fredenslund, A.; Schiller, M.; Gmehling, J. Vapor-liquid equilibria by UNIFAC group contribution. 5. Revision and extension. *Ind. Eng. Chem. Res.* **1991**, *30* (10), 2352−2355.
(45) Petters, M. D.; Kreidenweis, S. M.; Prenni, A. J.; Sullivan, R. C.; Carrico, C. M.; Koehler, K. A.; Ziemann, P. J. Role of molecular size in cloud droplet activation. *Geophys. Res. Lett.* **2009**, *36* (22), L22801.
(46) Bilde, M.; Barsanti, K.; Booth, M.; Cappa, C. D.; Donahue, N. M.; Emanuelsson, E. U.; McFiggans, G.; Krieger, U. K.; Marcolli, C.; Topping, D.; et al. Saturation vapor pressures and transition enthalpies of low-volatility organic molecules of atmospheric relevance: From dicarboxylic acids to complex mixtures. *Chem. Rev.* **2015**, *115* (10), 4115−4156.
(47) Zuend, A.; Seinfeld, J. H. Modeling the gas-particle partitioning of secondary organic aerosol: The importance of liquid-liquid phase separation. *Atmos. Chem. Phys.* **2012**, *12* (9), 3857−3882.
(48) Prausnitz, J. M.; Lichtenthaler, R. N.; de Azevedo, E. G. *Molecular Thermodynamics of Fluid-Phase Equilibria*, 3rd ed.; Prentice Hall: Upper Saddle River, NJ, 1999.
(49) Petters, M. D.; Kreidenweis, S. M.; Snider, J. R.; Koehler, K. A.; Wang, Q.; Prenni, A. J.; DeMott, P. J. Cloud droplet activation of polymerized organic aerosol. *Tellus, Ser. B* **2006**, *58* (3), 196−205.
(50) Tobias, H. J.; Ziemann, P. J. Compound identification in organic aerosols using temperature-programmed thermal desorption particle beam mass spectrometry. *Anal. Chem.* **1999**, *71* (16), 3428−3435.
(51) Tobias, H. J.; Kooiman, P. M.; Docherty, K. S.; Ziemann, P. J. Real-time chemical analysis of organic aerosols using a thermal desorption particle beam mass spectrometer. *Aerosol Sci. Technol.* **2000**, *33* (1−2), 170−190.
(52) Ranney, A. P.; Ziemann, P. J. Identification and quantification of oxidized organic aerosol compounds using derivatization, liquid chromatography, and chemical ionization mass spectrometry. *Aerosol Sci. Technol.* **2017**, *51*, 342.
(53) Moore, R. H.; Nenes, A. Scanning flow CCN analysis — a method for fast measurements of CCN spectra. *Aerosol Sci. Technol.* **2009**, *43* (12), 1192−1207.
(54) Moore, R. H.; Nenes, A.; Medina, J. Scanning mobility CCN analysis—a method for fast measurements of size-resolved CCN distributions and activation kinetics. *Aerosol Sci. Technol.* **2010**, *44* (10), 861−871.
(55) Petters, S. S.; Petters, M. D. Surfactant effect on cloud condensation nuclei for two-component internally mixed aerosols. *J. Geophys. Res. -Atmos.* **2016**, *121* (4), 1878−1895.
(56) Roberts, G. C.; Nenes, A. A continuous-flow streamwise thermal-gradient CCN chamber for atmospheric measurements. *Aerosol Sci. Technol.* **2005**, *39* (3), 206−221.
(57) Clegg, S. L.; Brimblecombe, P.; Wexler, A. S. Thermodynamic model of the system H^+− NH_4^+− Na^+− SO_4^{2-}− NO_3^-− Cl^-− H_2O at 298.15 K. *J. Phys. Chem. A* **1998**, *102* (12), 2155−2171.
(58) Wexler, A. S.; Clegg, S. L. Atmospheric aerosol models for systems including the ions H^+, NH_4^+, Na^+, SO_4^{2-}, NO_3^-, Cl^-, Br^-, and H_2O. *J. Geophys. Res.* **2002**, *107* (D14), 4207.
(59) Rose, D.; Gunthe, S. S.; Mikhailov, E.; Frank, G. P.; Dusek, U.; Andreae, M. O.; Pöschl, U. Calibration and measurement uncertainties of a continuous-flow cloud condensation nuclei counter (DMT-CCNC): CCN activation of ammonium sulfate and sodium chloride aerosol particles in theory and experiment. *Atmos. Chem. Phys.* **2008**, *8* (5), 1153−1179.
(60) Nguyen, T. K. V.; Petters, M. D.; Suda, S. R.; Guo, H.; Weber, R. J.; Carlton, A. G. Trends in particle-phase liquid water during the Southern Oxidant and Aerosol Study. *Atmos. Chem. Phys.* **2014**, *14* (20), 10911−10930.

DOI: 10.1021/acs.jpca.7b04114
J. Phys. Chem. A 2017, 121, 5164−5174

(61) Petters, M. D.; Carrico, C. M.; Kreidenweis, S. M.; Prenni, A. J.; DeMott, P. J.; Collett, J. L., Jr.; Moosmüller, H. Cloud condensation nucleation activity of biomass burning aerosol. *J. Geophys. Res.* **2009**, *114*, D22205.
(62) Suda, S. R.; Petters, M. D. Accurate determination of aerosol activity coefficients at relative humidities up to 99% using the hygroscopicity tandem differential mobility analyzer technique. *Aerosol Sci. Technol.* **2013**, *47* (9), 991−1000.
(63) Dawson, K. W.; Petters, M. D.; Meskhidze, N.; Petters, S. S.; Kreidenweis, S. M. Hygroscopic growth and cloud droplet activation of xanthan gum as a proxy for marine hydrogels. *J. Geophys. Res. Atmos.* **2016**, *121* (19), 11803−11818.
(64) Wright, T. P.; Song, C.; Sears, S.; Petters, M. D. Thermodynamic and kinetic behavior of glycerol aerosol. *Aerosol Sci. Technol.* **2016**, *50* (12), 1385−1396.
(65) Rader, D. J.; McMurry, P. H. Application of the tandem differential mobility analyzer to studies of droplet growth or evaporation. *J. Aerosol Sci.* **1986**, *17* (5), 771−787.
(66) Rothfuss, N. E.; Petters, M. D. Coalescence-based assessment of aerosol phase state using dimers prepared through a dual-differential mobility analyzer technique. *Aerosol Sci. Technol.* **2016**, *50* (12), 1294−1305.
(67) Stolzenburg, M.; Kreisberg, N.; Hering, S. Atmospheric size distributions measured by differential mobility optical particle size spectrometry. *Aerosol Sci. Technol.* **1998**, *29* (5), 402−418.
(68) Marcolli, C.; Peter, T. Water activity in polyol/water systems: New UNIFAC parameterization. *Atmos. Chem. Phys.* **2005**, *5* (6), 1545−1555.
(69) Schwarzenbach, R. P.; Gschwend, P. M.; Imboden, D. M. *Environmental Organic Chemistry*, 1st ed.; John Wiley & Sons: New York, 1993.
(70) Bilde, M.; Svenningsson, B.; Mønster, J.; Rosenørn, T. Even−odd alternation of evaporation rates and vapor pressures of C3−C9 dicarboxylic acid aerosols. *Environ. Sci. Technol.* **2003**, *37* (7), 1371−1378.
(71) Frosch, M.; Zardini, A. A.; Platt, S. M.; Müller, L.; Reinnig, M.-C.; Hoffmann, T.; Bilde, M. Thermodynamic properties and cloud droplet activation of a series of oxo-acids. *Atmos. Chem. Phys.* **2010**, *10* (13), 5873−5890.
(72) Thalladi, V. R.; Boese, R.; Weiss, H.-C. The melting point alternation in α,ω-alkanedithiols. *J. Am. Chem. Soc.* **2000**, *122* (6), 1186−1190.
(73) Thalladi, V. R.; Nüsse, M.; Boese, R. The melting point alternation in α,ω-alkanedicarboxylic acids. *J. Am. Chem. Soc.* **2000**, *122* (38), 9227−9236.
(74) Matsunaga, A.; Ziemann, P. J. Yields of β-hydroxynitrates, dihydroxynitrates, and trihydroxynitrates formed from OH radical-initiated reactions of 2-methyl-1-alkenes. *Proc. Natl. Acad. Sci. U. S. A.* **2010**, *107* (15), 6664−6669.
(75) Matsunaga, A.; Ziemann, P. J. Yields of β-hydroxynitrates and dihydroxynitrates in aerosol formed from OH radical-initiated reactions of linear alkenes in the presence of NO_x. *J. Phys. Chem. A* **2009**, *113* (3), 599−606.
(76) Algrim, L. B.; Ziemann, P. J. Effect of the keto group on yields and composition of organic aerosol formed from OH radical-initiated reactions of ketones in the presence of NO_x. *J. Phys. Chem. A* **2016**, *120* (35), 6978−6989.
(77) Diller, D. E.; Van Poolen, L. J. Measurements of the viscosities of saturated and compressed liquid normal butane and isobutane. *Int. J. Thermophys.* **1985**, *6* (1), 43−62.
(78) Rothfuss, N. E.; Petters, M. D. Influence of functional groups on the viscosity of organic aerosol. *Environ. Sci. Technol.* **2017**, *51* (1), 271−279.
(79) Bailey, P. S. The reactions of ozone with organic compounds. *Chem. Rev.* **1958**, *58* (5), 925−1010.
(80) Murai, S.; Sonoda, N.; Tsutsumi, S. The redox reaction of 1-ethoxy-n-heptyl hydroperoxide. *Bull. Chem. Soc. Jpn.* **1964**, *37* (8), 1187−1190.
(81) Tobias, H. J.; Ziemann, P. J. Thermal desorption mass spectrometric analysis of organic aerosol formed from reactions of 1-tetradecene and O_3 in the presence of alcohols and carboxylic acids. *Environ. Sci. Technol.* **2000**, *34* (11), 2105−2115.
(82) Bilde, M.; Svenningsson, B. CCN activation of slightly soluble organics: The importance of small amounts of inorganic salt and particle phase. *Tellus, Ser. B* **2004**, *56* (2), 128−134.
(83) Kristensson, A.; Rosenørn, T.; Bilde, M. Cloud droplet activation of amino acid aerosol particles. *J. Phys. Chem. A* **2010**, *114* (1), 379−386.
(84) Wex, H.; Stratmann, F.; Topping, D.; McFiggans, G. The Kelvin versus the Raoult term in the Köhler equation. *J. Atmos. Sci.* **2008**, *65* (12), 4004−4016.
(85) Facchini, M. C.; Mircea, M.; Fuzzi, S.; Charlson, R. J. Cloud albedo enhancement by surface-active organic solutes in growing droplets. *Nature* **1999**, *401* (6750), 257−259.
(86) Giordano, M. R.; Short, D. Z.; Hosseini, S.; Lichtenberg, W.; Asa-Awuku, A. Changes in droplet surface tension affect the observed hygroscopicity of photochemically aged biomass burning aerosol. *Environ. Sci. Technol.* **2013**, *47* (19), 10980−10986.
(87) Nozière, B.; Baduel, C.; Jaffrezo, J.-L. The dynamic surface tension of atmospheric aerosol surfactants reveals new aspects of cloud activation. *Nat. Commun.* **2014**, *5*, 3333.
(88) Li, Z.; Williams, A. L.; Rood, M. J. Influence of soluble surfactant properties on the activation of aerosol particles containing inorganic solute. *J. Atmos. Sci.* **1998**, *55* (10), 1859−1866.
(89) Sorjamaa, R.; Svenningsson, B.; Raatikainen, T.; Henning, S.; Bilde, M.; Laaksonen, A. The role of surfactants in Köhler theory reconsidered. *Atmos. Chem. Phys.* **2004**, *4* (8), 2107−2117.
(90) Prisle, N. L.; Raatikainen, T.; Sorjamaa, R.; Svenningsson, B.; Laaksonen, A.; Bilde, M. Surfactant partitioning in cloud droplet activation: A study of C8, C10, C12 and C14 normal fatty acid sodium salts. *Tellus, Ser. B* **2008**, *60* (3), 416−431.
(91) Kristensen, T. B.; Wex, H.; Nekat, B.; Nøjgaard, J. K.; van Pinxteren, D.; Lowenthal, D. H.; Mazzoleni, L. R.; Dieckmann, K.; Koch, C. B.; Mentel, T. F.; et al. Hygroscopic growth and CCN activity of HULIS from different environments. *J. Geophys. Res. Atmos.* **2012**, *117*, D22203.
(92) Petters, M. D.; Suda, S. R.; Christensen, S. I. The role of dynamic surface tension in cloud droplet activation. *AIP Conf. Proc.* **2013**, *1527* (1), 801−807.
(93) Bzdek, B. R.; Power, R. M.; Simpson, S. H.; Reid, J. P.; Royall, C. P. Precise, contactless measurements of the surface tension of picolitre aerosol droplets. *Chem. Sci.* **2016**, *7* (1), 274−285.
(94) Raatikainen, T.; Laaksonen, A. A simplified treatment of surfactant effects on cloud drop activation. *Geosci. Model Dev.* **2011**, *4* (1), 107−116.
(95) Ruehl, C. R.; Davies, J. F.; Wilson, K. R. An interfacial mechanism for cloud droplet formation on organic aerosols. *Science* **2016**, *351* (6280), 1447.
(96) Petters, M. D.; Kreidenweis, S. M. A single parameter representation of hygroscopic growth and cloud condensation nucleus activity − Part 3: Including surfactant partitioning. *Atmos. Chem. Phys.* **2013**, *13* (2), 1081−1091.
(97) Renbaum-Wolff, L.; Grayson, J. W.; Bateman, A. P.; Kuwata, M.; Sellier, M.; Murray, B. J.; Shilling, J. E.; Martin, S. T.; Bertram, A. K. Viscosity of α-pinene secondary organic material and implications for particle growth and reactivity. *Proc. Natl. Acad. Sci. U. S. A.* **2013**, *110* (20), 8014−8019.
(98) Asa-Awuku, A.; Engelhart, G. J.; Lee, B. H.; Pandis, S. N.; Nenes, A. Relating CCN activity, volatility, and droplet growth kinetics of β-caryophyllene secondary organic aerosol. *Atmos. Chem. Phys.* **2009**, *9* (3), 795−812.
(99) Ortiz-Montalvo, D.; Lim, Y. B.; Perri, M. J.; Seitzinger, S. P.; Turpin, B. J. Volatility and yield of glycolaldehyde SOA formed through aqueous photochemistry and droplet evaporation. *Aerosol Sci. Technol.* **2012**, *46* (9), 1002−1014.
(100) Ortiz-Montalvo, D.; Häkkinen, S. A. K.; Schwier, A. N.; Lim, Y. B.; McNeill, V. F.; Turpin, B. J. Ammonium addition (and aerosol pH)

DOI: 10.1021/acs.jpca.7b04114
J. Phys. Chem. A 2017, 121, 5164−5174

has a dramatic impact on the volatility and yield of glyoxal secondary organic aerosol. *Environ. Sci. Technol.* **2014**, *48* (1), 255−262.
(101) Topping, D.; Connolly, P.; McFiggans, G. Cloud droplet number enhanced by co-condensation of organic vapours. *Nat. Geosci.* **2013**, *6* (6), 443−446.
(102) Nakao, S.; Suda, S. R.; Camp, M.; Petters, M. D.; Kreidenweis, S. M. Droplet activation of wet particles: Development of the wet CCN approach. *Atmos. Meas. Technol.* **2014**, *7* (7), 2227−2241.
(103) Lee, A. K. Y.; Ling, T. Y.; Chan, C. K. Understanding hygroscopic growth and phase transformation of aerosols using single particle Raman spectroscopy in an electrodynamic balance. *Faraday Discuss.* **2008**, *137* (0), 245−263.
(104) Hilal, S. H.; Karickhoff, S. W.; Carreira, L. A. Prediction of the vapor pressure boiling point, heat of vaporization and diffusion coefficient of organic compounds. *QSAR Comb. Sci.* **2003**, *22* (6), 565−574.
(105) Minkoff, G. J. The infra-red absorption spectra of organic peroxides. *Proc. R. Soc. London, Ser. A* **1954**, *224* (1157), 176−191.
(106) Johnson, R. M.; Siddiqi, I. W. *The Determination of Organic Peroxides*; Pergamon: Oxford, 1970; Vol. *4*, p 119.
(107) Yablonskii, O. P.; Belyaev, V. A.; Vinogradov, A. N. Association of hydrocarbon hydroperoxides. *Russ. Chem. Rev.* **1972**, *41* (7), 565−573.
(108) Barley, M. H.; Topping, D. O.; McFiggans, G. Critical assessment of liquid density estimation methods for multifunctional organic compounds and their use in atmospheric science. *J. Phys. Chem. A* **2013**, *117* (16), 3428−3441.
(109) Kurtén, T.; Tiusanen, K.; Roldin, P.; Rissanen, M.; Luy, J.-N.; Boy, M.; Ehn, M.; Donahue, N. α-pinene autoxidation products may not have extremely low saturation vapor pressures despite high O:C ratios. *J. Phys. Chem. A* **2016**, *120* (16), 2569−2582.

DOI: 10.1021/acs.jpca.7b04114
J. Phys. Chem. A 2017, 121, 5164−5174